

## **REMARKS**

### **Overview of the Office Action**

Claims 1, 14, 104, 112, and 116 have been rejected under 35 U.S.C. §103(a) as unpatentable over U.S. Patent No. 6,834,036 (“Shiono”) in view of U.S. Patent No. 6,870,805 (“Arai”), and in further view of U.S. Patent No. 6,594,222 (“Maruyama”).

Claims 105, 106, 117, and 118 have been rejected under 35 U.S.C. §103(a) as unpatentable over Shiono in view of Arai, and further in view of U.S. Patent No. 6,807,019 (“Takeuchi”).

### **Status of the claims**

Claims 2-10, 12-13, 45-50, 99, 102, 103, 111, 114, 115, and 123 have been previously canceled.

Claims 11, 15-44, 51-98, 100-101, 107-110, 113, and 119-122 have been previously withdrawn.

Claim 11 is amended to correct the dependency thereof. Upon allowance of independent claim 1, consideration of claim 11 is requested.

Claims 1, 14, 104-106, 112, and 116-118 remain pending.

### **Rejection of claims 1, 14, 104, 112, and 116 under 35 U.S.C. §103(a)**

The Office Action states that the combination of Shiono and Arai teaches all of Applicants’ recited elements.

Independent claim 1 recites, in part, an optical pickup apparatus “wherein the diffraction order number of the light flux of the wavelength  $\lambda_3$  having passed the different diffractive

structure is different from the diffraction order number of the light flux of the wavelength  $\lambda_3$  having passed the first diffractive structure”, which Shiono, Arai, and Maruyama fail to teach or suggest.

The Examiner concedes that Shiono and Arai both fail to teach or suggest the above-mentioned limitation. However, the Examiner cites Fig. 3a and col. 11, lines 25-54 of Maruyama as teaching Applicants’ recited limitation. Applicants submit that Maruyama has been misunderstood.

Maruyama discloses an objective lens of an optical pick-up. The objective lens includes a refractive lens and a diffractive lens structure that is formed as a large number of concentric ring areas having minute steps in an optical axis direction at the boundaries therebetween (see Figs 1a and 1b of Maruyama).

The lens surface of the objective lens of Maruyama is divided into a high numerical aperture (NA) exclusive area (RE) (used for a DVD only), and a common area (RC) surrounded by the high NA exclusive area (RE) (see col. 5, lines 53-64). The diffractive lens structure of Maruyama in the common area changes the spherical aberration in the undercorrected direction as the wavelength of the incident laser beam increases (see col. 6, lines 52-59). The diffractive lens structure of Maruyama formed in the high NA exclusive area (RE) has a smaller wavelength dependence of a spherical aberration than that formed in the common area (RC), and is designed such that a spherical aberration at the short wavelength is adequately corrected for the thin cover type optical disc, such as a CD (see col. 7, lines 5-10 and the abstract of Maruyama).

The passages of Maruyama cited by the Examiner simply disclose that the lens (10) of Maruyama includes a first surface (11) and a second surface (12), and that first surface (11) of Maruyama includes a common area surrounded by the high NA exclusive area. The cited

passages of Maruyama also describe the various coefficients that define the base curve and the diffractive lens structure of the common area (RC) of the first surface (11), the various coefficients that define the base curve and the diffractive lens structure of the high NA exclusive area (RE) of the first surface (11), and the various coefficients that define the second surface (12). An equation used to define the rotationally-symmetrical aspherical surface of the lens of Maruyama is also disclosed.

As we previously argued, the Examiner-cited passages of Maruyama fail to teach or suggest that the diffraction order number of the light flux of the wavelength  $\lambda_3$  having passed the different diffractive structure is different from the diffraction order number of the light flux of the wavelength  $\lambda_3$  having passed the first diffractive structure, as recited in Applicants' claim 1.

The following paragraphs reiterate the arguments previously presented and further include our comments to the Examiner's response to the previous argument.

As is known to those skilled in the art, the order number of diffracted light  $m$ , can be calculated using the following formula,

$$m = (n-1) \times d_s / \lambda;$$

where  $m$  is the order number,  $n$  is the refractive index of the optical element,  $d_s$  is the distance of the minute step in the direction of the optical axis, and  $\lambda$  is the wavelength of the incident light flux. The veracity of this formula as it relates the presently claimed optical element is described in detail below.

As is also known by those skilled in the art, if the order number  $m$  is between 0.51 and 1.49, the order number  $m$  is deemed to be 1. Further, if the order number  $m$  is between 1.51 and 2.49, order number  $m$  is deemed to be 2.

Using the above formula and the values disclosed in Table 1 (first embodiment) and Table 3 (second embodiment) of Maruyama, the various order numbers  $m$  can be calculated, and are shown in the table below.

Embodiment of Maruyama	Index of refraction ( $n$ )	$\lambda$	$d_s$ for RC	Order number ( $m$ ) of the light flux of common area (RC)	$d_s$ for RE	Order number ( $m$ ) of the light flux of High-NA exclusive area (RE)
1 <sup>st</sup> Embodiment (col. 11, line 25 to col. 12, line 40; table 1)	1.54059	656 nm	1337.2 nm	1 (1.102)	1215.4 nm	1 (1.002)
1 <sup>st</sup> Embodiment	1.53653	790 nm	1337.2 nm	1 (0.908)	1215.4 nm	1 (0.825)
2 <sup>nd</sup> Embodiment (col. 14, line 45 to col. 15, line 25; table 3)	1.54048	659 nm	1340 nm	1 (1.099)	1223.7 nm	1 (1.004)
2 <sup>nd</sup> Embodiment	1.53653	790 nm	1340 nm	1 (0.910)	1223.7 nm	1 (0.831)

The above table shows that, in both embodiments of Maruyama, the diffraction order number  $m$  of the light flux that has passed through a diffractive structure of the common area (RC) is same as the diffraction order number  $m$  of the light flux that has passed through a diffractive structure of the high-NA exclusive area (RE).

In contrast to Maruyama, Applicants' amended claim 1 clearly recites "wherein the diffraction order number of the light flux of the wavelength  $\lambda_3$  having passed the different diffractive structure is different from the diffraction order number of the light flux of the wavelength  $\lambda_3$  having passed the first diffractive structure". Therefore, Maruyama clearly fails

to teach or suggest the elements of Applicants' independent claim 1 that Shiono and Arai are missing.

In response to the above argument, the Examiner asserts that "Maruyama discloses in Table 1 the coefficients that are associated with each of the orders and their values for each of the regions of the lens (i.e.  $P_{2c}$ ,  $P_{2e}$  are the coefficients for second order light, see col. 9 lines 16-39)", that "these coefficients are related to the optical path difference which is caused by the corresponding section of the lens and affects the order of light which exits the lens", and that "it is clear from Table 1 the coefficients have different values for the different regions, and therefore the order numbers are different for the different regions."

Applicants' submit that the Examiner has misunderstood the teachings of Maruyama.

$P_{2c}$ ,  $P_{2e}$  shown in Table 1 of Maruyama are the coefficients of second "orders" of optical path difference function  $\Phi c(h)$ , and not the coefficients for second "order" light flux, as recited in Applicants' claim 1.

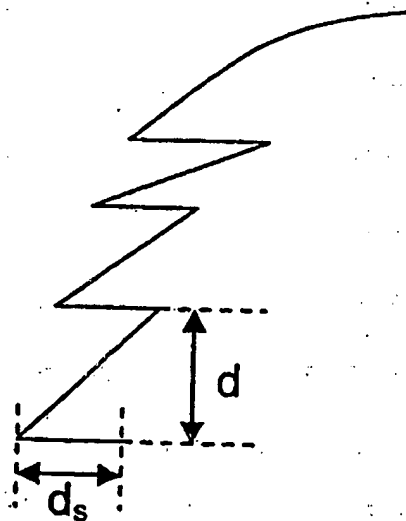
The English translation of Maruyama is not a strictly correct translation. Specifically,  $P_{2c}$ ,  $P_{2e}$  in Table 1 of Maruyama should have been translated to refer to the coefficients of second "power" of optical path difference function  $\Phi c(h)$ .

The diffraction order number cannot be obtained from  $P_{2c}$ ,  $P_{2e}$  in Table 1. Therefore, table 1 of Maruyama fails to disclose the coefficients that are associated with each of the diffraction orders and their values for each of the regions of the lens.

The Examiner further asserts that "the correct formula for modeling diffraction is  $n_2 \sin \Theta_2 - n_1 \sin \Theta_1 = (M\lambda)/d = M\lambda T$ " and that Applicants' equation  $m = (n-1) d_s / \lambda$  is incorrect.

The following explains why  $n_2 \sin \Theta_2 - n_1 \sin \Theta_1 = (M\lambda)/d = M\lambda T$  is not the formula for diffraction for the presently claimed optical element and shows why the equation  $m = (n-1) d_s / \lambda$  presented by Applicant is correct for the presently claimed optical element.

First, the “d” in the equation  $n_2 \sin \Theta_2 - n_1 \sin \Theta_1 = (M\lambda)/d$  of Maruyama is different from the  $d_s$  in Applicants’ equation  $m = (n-1) d_s / \lambda$ . More specifically, the d in the equation of Maruyama is the line spacing of the diffractive structure, which is a length between one step of the diffractive structure and next step of the diffractive structure in a direction perpendicular to the optical axis. In contrast, the  $d_s$  in Applicants’ equation is a length of one step of the diffractive structure in the direction of the optical axis (see the Figure below). Hence the d in the equation of Maruyama is completely different from the  $d_s$  in Applicants’ equation. Accordingly, the equation  $n_2 \sin \Theta_2 - n_1 \sin \Theta_1 = (M\lambda)/d$  of Maruyama cannot be considered to be the formula for modeling diffraction for the presently claimed optical element.



Further, the equation  $n_2 \sin \Theta_2 - n_1 \sin \Theta_1 = (M\lambda)/d$  cannot be applied to the diffractive structure of Maruyama because this formula can only be applied to a diffractive structure having steps at equal intervals in a direction perpendicular to the optical axis, which is not true of the diffractive structure of Maruyama. In other words, the intervals between the steps of the diffractive structure of Maruyama are not equal (see Fig. 3A of Maruyama). Instead, the diffractive order of a diffractive structure having steps at intervals that are not equal is calculated using equation  $m = (n-1) d_s / \lambda$ .

Applicants' argument is supported by a thesis "Harmonic diffractive lenses" from APPLIED OPTICS, a copy of which is attached hereto.

According to the attached thesis, the lens on the left of Fig. 1 in page 2470 shows a diffractive lens generating a first diffraction order light flux. The lens on the right of Fig. 1 shows a diffractive lens generating high diffraction order light flux.

Fig. 1 of the attached thesis shows that  $d_s = m \lambda_0 / (n-1)$ . Therefore, Fig. 1 confirms that  $m = (n-1) d_s / \lambda_0$ , where  $d_s$  is a length of one step of the diffractive structure in a direction of the optical axis,  $m$  is a diffraction order number,  $\lambda_0$  is a wavelength of a light flux, and  $n$  is a refractive index of the lens. Consequently, that attached thesis confirms that the equation  $m = (n-1) d_s / \lambda$  used in Applicants' arguments is, in fact, correct for the presently claimed optical element.

Accordingly, the order number of light shown in the table above is technically correct. In each of the examples disclosed by Maruyama, diffraction order number of light flux that has passed through a diffractive structure of a common area is the same as the diffraction order number of the light flux that has passed through a diffractive structure of high-NA exclusive area.

Therefore, Maruyama fails to teach or suggest an optical pickup apparatus “wherein the diffraction order number of the light flux of the wavelength  $\lambda_3$  having passed the different diffractive structure is different from the diffraction order number of the light flux of the wavelength  $\lambda_3$  having passed the first diffractive structure”, as recited in Applicants’ independent claim 1. Consequently, Maruyama fails to teach the elements of Applicants’ independent claim 1 that Shiono and Arai are missing.

In view of the foregoing, Shiono, Arai, and Maruyama, whether taken alone or in combination, fail to teach or suggest the subject matter recited in Applicants’ amended independent claim 1. Accordingly, claim 1 is patentable over Shiono, Arai, and Maruyama under 35 U.S.C. §103(a).

Independent claim 112 recites limitations similar to independent claim 1 and is therefore deemed to be patentably distinct over Shiono, Arai, and Maruyama for reasons discussed above with respect to independent claim 1.

#### Dependent claims

Claims 14, 104, and 116 have been canceled. Claims 14, 104, and 116 which depend from respective independent claims 1 and 112, respectively incorporate all of the limitations of independent claims 1 or 112 and are therefore deemed to be patentably distinct over Shiono, Arai, and Maruyama for at least those reasons discussed above with respect to independent claims 1 and 112.



Rejection of claims 105, 106, 117, and 118 under 35 U.S.C. §103(a)

The Office Action states that the combination of Shiono, Arai, and Takeuchi teaches all of Applicants' recited elements.

Shiono and Arai have been previously discussed, and do not teach or suggest the invention recited in Applicants' amended independent claims 1 and 112.

Because Shiono and Arai do not teach or suggest the subject matter recited in Applicants' amended independent claim 1, and because Takeuchi does not teach or suggest the elements of claim 1 that Shiono and Arai are missing, the addition of Takeuchi does not remedy the above-discussed deficiencies of Shiono and Arai.


Claims 105, 106, 117, and 118, which depend from independent claims 1 and 112, incorporate all of the limitations of the respective independent claim and are, therefore, patentably distinct over Shiono, Arai, and Takeuchi for at least those reasons discussed with respect to independent claims 1 and 112.

Conclusion

In view of the foregoing, reconsideration and withdrawal of all rejections, and allowance of all pending claims is respectfully solicited.

Should the Examiner have any comments, questions, suggestions, or objections, the Examiner is respectfully requested to telephone the undersigned in order to facilitate reaching a resolution of any outstanding issues.

Respectfully submitted,  
COHEN PONTANI LIEBERMAN & PAVANE LLP

By   
Alfred W. Froehrich  
Reg. No. 38,887  
551 Fifth Avenue, Suite 1210  
New York, New York 10176  
(212) 687-2770

Dated: December 23, 2008

# Harmonic diffractive lenses

Donald W. Sweeney and Gary E. Sommargren

The harmonic diffractive lens is a diffractive imaging lens for which the optical path-length transition between adjacent facets is an integer multiple  $m$  of the design wavelength  $\lambda_0$ . The total lens thickness in air is  $m\lambda_0/(n-1)$ , which is  $m$  times thicker than the so-called modulo  $2\pi$  diffractive lens. Lenses constructed in this way have hybrid properties of both refractive and diffractive lenses. Such a lens will have a diffraction-limited, common focus for a number of discrete wavelengths across the visible spectrum. A 34.75-diopter, 6-mm-diameter lens is diamond turned in aluminum and replicated in optical materials. The sag of the lens is 23  $\mu\text{m}$ . Modulation transfer function measurements in both monochromatic and white light verify the performance of the lens. The lens approaches the diffraction limit for 10 discrete wavelengths across the visible spectrum.

## 1. Introduction

A single-element diffractive lens that focuses many wavelengths to the same axial location would have numerous applications. An imaging lens would have the often-stated advantages of diffractive optics, such as being thin, lightweight, and inexpensive when mass produced. Unfortunately, a diffractive lens tends to exhibit large chromatic aberrations and, frequently, low diffraction efficiency. The diffraction efficiency can in principle be increased to 100% with proper blazing. The chromatic aberrations, however, are more difficult to correct. Across the visible spectrum, for example, a normal diffractive lens that reconstructs in first order introduces  $\sim 1$  diopter of axial chromatic aberration for every 3 diopters of power. In this paper we discuss methods for overcoming the chromatic variation of focal length at a discrete number of wavelengths while preserving the microthin character of diffractive optics.

We show here that a single-element diffractive lens with multiwavelength path-length steps, rather than a single-wavelength step, has the same optical power for a number of discrete harmonic wavelengths. Elements of this type were recently introduced independently by Sweeney and Sommargren<sup>1</sup> and Morris and Faklis.<sup>2</sup> Lenses constructed in this way have hybrid properties of both refractive and diffractive

lenses. These lenses, which we call harmonic diffractive lenses, have multiple facets of equal area. Each facet has a constant optical path-length delay with respect to its neighbor.<sup>3</sup> At a number of wavelengths across the visible, this path-length delay is an integer number of wavelengths. At these wavelengths, the facets add constructively, and the resolution is equal to the resolution associated with the full aperture. At intermediate wavelengths, there are multiple spherical waves produced by the optic that are focused at axial locations other than the nominal focal plane. The axial spread of focal positions (which yields a defocusing aberration in the nominal focal plane) can be decreased if the step size is increased.

Single- and multiple-element diffractive lenses for broadband imaging are discussed extensively in the literature; see the reviews in Ref. 3 or Ref. 4. Buralli and Morris<sup>5</sup> give a good example of the performance degradation of a purely diffractive landscape lens as a function of source bandwidth. Bennett<sup>6</sup> and Sweatt<sup>7</sup> have shown that a purely diffractive, achromatic lens is possible, but only if it is a three-element diffractive system of negative power. The development of the harmonic diffractive lens described here uses the paraxial approximation, and geometric aberrations are not considered; the generalization to include geometric aberrations is straightforward.

## 2. Properties of the Harmonic Diffractive Lens

Figure 1 illustrates the difference between a blazed diffractive lens and what we call the harmonic diffractive lens. The lenses differ in step height and location. In the former case, the facets of the lens are arranged to introduce a  $2\pi$  phase shift at a selected

The authors are with Lawrence Livermore National Laboratory, University of California, Livermore, California 94550.

Received 19 August 1994; revised manuscript received 21 November 1994.

0003-6935/95/142469-07\$06.00/0

© 1995 Optical Society of America.

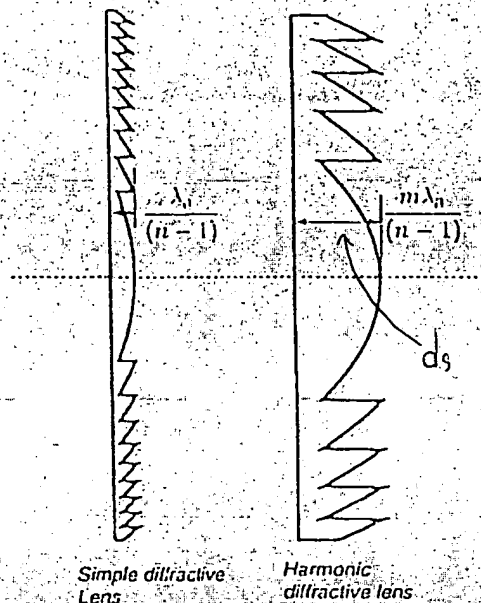


Fig. 1. Blazed diffractive lenses. The lens on the left is the thin-limit case and is referred to here as a simple diffractive lens or modulo  $2\pi$  diffractive lens. The lens on the right is a harmonic diffractive lens; it is a generalization of the modulo  $2\pi$  diffractive lens.

reference wavelength. The basic problem with using such a  $2\pi$  phase-shift diffractive lens for broad-band imaging is that optical power  $P$  depends linearly on wavelength. For example, the power of such a lens in air is

$$P \equiv \frac{1}{f} = \frac{k\lambda}{r_1^2} \quad \text{so that} \quad \frac{\Delta P}{P} = \frac{\Delta \lambda}{\lambda}, \quad (1)$$

where  $f$  is the focal length in meters,  $k$  is the diffracted order,  $\lambda$  is wavelength, and  $r_1$  is the radius of the first Fresnel zone. A diffractive lens of 20-diopter power at 550 nm shifts to 14.5 diopters at a wavelength of 400 nm and 25.5 diopters at 700 nm.

The dispersive spread can be reduced by the use of the thickness of the lens as a degree of freedom. The thickness  $t$  of either blazed lens shown in Fig. 1 as a function of radius  $r$  is given by

$$t(r, \lambda_0) = \left( \frac{-1}{\Delta n} \right) \text{MOD}_{m\lambda_0} \left( \frac{r^2}{2f} \right), \quad m = 1, 2, 3, 4, \quad (2)$$

$$\Delta n \equiv (n - 1),$$

where  $\lambda_0$  is the central design wavelength and  $n$  is the refractive index of the lens. Generalization to an arbitrary  $m$  ( $m = 2, 3, 4, \dots$ ) is the definition of a harmonic diffractive lens. Increasing values of  $m$  represent the progression from the simple diffractive lens ( $m = 1$ ) with path-length steps of  $\lambda_0/\Delta n$  to a harmonic diffractive lens with path-length steps of  $m\lambda_0/\Delta n$  through to a purely refractive lens, with the final thickness reached with the first cut equal to the radius of the lens.

To understand the effect of  $m$  in Eq. (2), think of

the harmonic diffractive lens as a simple diffractive lens made for an effective wavelength  $\lambda_{\text{eff}} = m\lambda_0$ . The optical path-length step  $m\lambda_0$  created by the modulus operation in Eq. (2) has resonant (or harmonic) wavelengths at  $m\lambda_0/k$ , i.e., at each of these wavelengths the phase change between adjacent steps of the lens is a multiple of  $2\pi$ . For example, if  $\lambda_0 = 550$  nm and  $m = 10$ , then the resonances in the visible are at 423, 459, 500, 550, 611, and 687 nm for  $k = 13, 12, 11, 10, 9$ , and 8 respectively.

If this lens is illuminated by  $\lambda_{\text{eff}}$  the lens will diffract 100% of the energy into the first diffracted order with a focal position given by Eq. (1). Fourier analysis of Eq. (2) also shows that the diffraction efficiency  $\eta$  of the lens at any wavelength is

$$\eta = \text{sinc}^2 \left( \frac{m\lambda_0}{\lambda} - k \right) \quad (3)$$

Thus, if the lens is illuminated by  $\lambda = \lambda_{\text{eff}}/k$ , the lens will again diffract 100% of its energy into the  $k$ th diffracted order. With Eq. (1), the  $k$ 's in the numerator cancel, leaving the power unchanged:

$$P = \frac{k(\lambda_{\text{eff}}/k)}{r_1^2} = \frac{\lambda_{\text{eff}}}{r_1^2} \quad (4)$$

This is depicted graphically in Fig. 2. If the lens is illuminated with any of the resonant wavelengths, each will form a diffraction-limited focus in the same axial plane. At wavelengths away from the resonant wavelengths, the focal positions for each order follow the grating equation, but the diffracted intensity falls quickly. To a good approximation ( $m > 5$ ), the dis-

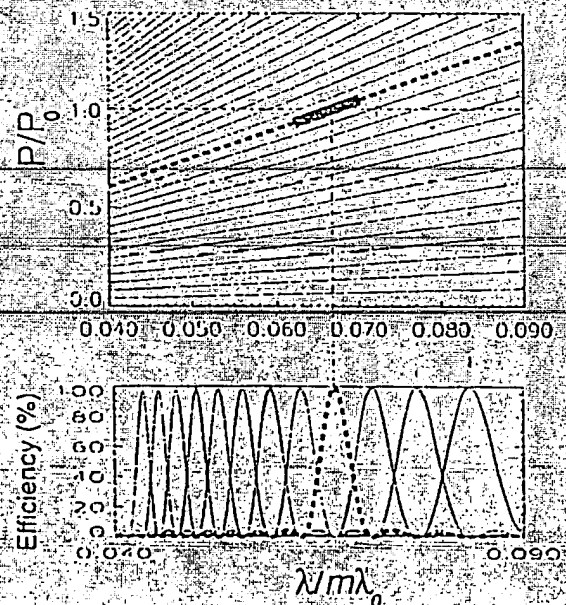


Fig. 2. Top panel shows the optical power of the diffracted orders from a harmonic diffractive lens as a function of wavelength; the bottom panel shows the diffraction efficiency as a function of wavelength for each order. An example of diffracted order (shown in bold) diffracts only significant light in the spectral region shown.



persive spread and thickness variations for the harmonic diffractive lens are

$$\frac{\Delta P}{P} = \frac{\Delta \lambda}{\lambda} = \frac{\lambda_0 - \frac{m\lambda_0}{(m+1)}}{\lambda_0} \approx \frac{1}{m} \quad \text{and} \quad \Delta l_{\max} = \frac{m\lambda_0}{\Delta n} \quad (5)$$

Physically, we are trading between the thickness of the diffractive lens and the achromatic performance. The important point is that at any resonant wavelength the focus is diffraction limited. At intermediate wavelengths, the focus has an axial spread that is symmetric about the nominal focal plane. Figure 3 is another visualization of the diffracted field for specific wavelengths and optical power. The lens was designed with  $m = 15$  for a design wavelength of 550 nm. Orders 12 to 21 reconstruct in the visible.

The lens can be interpreted physically if Eq. (2) is rewritten as

$$l(r, \lambda_0) = \left( \frac{1}{\Delta n} \right) \frac{r^2}{2f} - \left( \frac{1}{\Delta n} \right) \text{FLOOR}_{m\lambda_0} \left[ \frac{r^2}{2f} \right], \quad m = 1, 2, 3, \dots \quad (6)$$

where

$$\text{FLOOR}_b(a) \equiv b \text{ INTEGER} \left( \frac{a}{b} \right),$$

and the INTEGER operator equals the largest integer contained in the argument. Equation (6) is represented in Fig. 4; the harmonic diffractive lens equals the refractive lens minus an echelon. We can identify the first term on the right-hand side of Eq. (6) as the refractive part and the second term as the diffractive part. The refractive term provides a correct (paraxial) spherical wave. The second term

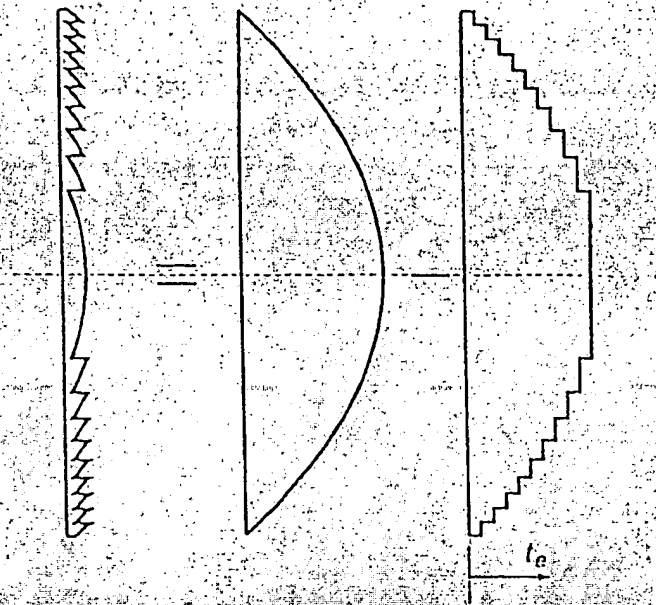


Fig. 4. Diffractive element on the left can be decomposed into the difference between the two elements on the right.

generates an additional diffraction grating term. As depicted in Fig. 5, the second term leads to a periodic phase function that modulates the spherical wave front. At the harmonic wavelengths  $m\lambda_0$ ,  $k$  the second term is a simple  $2\pi$ . At all other wavelengths, it is a binary phase grating, as shown in Fig. 5. One need only apply their knowledge of binary gratings to understand the impact of the phase modulation. For example, midway between two harmonic wavelengths the grating is a binary phase grating with a  $\pi$  phase shift. This splits the spherical wave associated with the refractive component into multiple spherical waves with 40.5% into each of the first orders, etc.

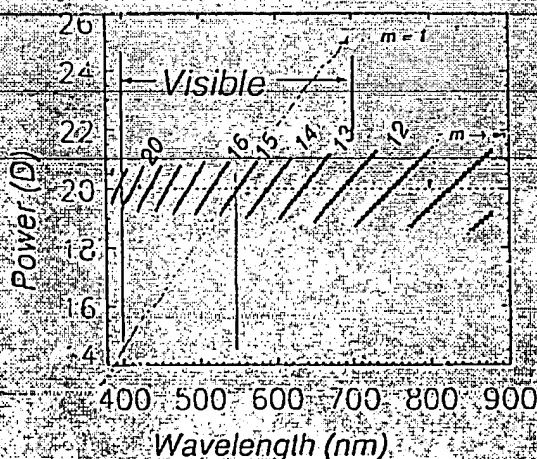


Fig. 3. Distribution of energy for the  $m = 15$  harmonic diffractive lens. Diffracted orders 12 to 21 (i.e.,  $k$  values) contribute to the focus across the visible. For a simple diffractive lens, the diffracted energy would be (to first order) distributed along the dashed line labeled  $m = 1$ .

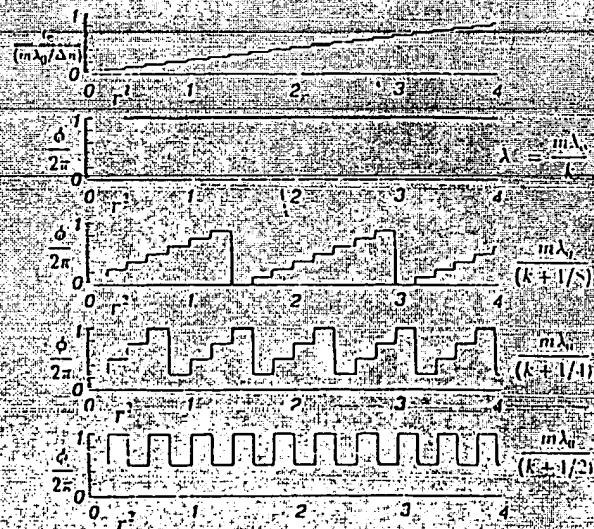


Fig. 5. Phase factor introduced by the echelon structure shown in Fig. 4 for various wavelengths.  $l_e$  is the echelon thickness shown in Fig. 4.

### 3. Simulation of Imaging Characteristics

Numerical simulations are used to compute the impulse response and the modulation transfer function (MTF) for resonant and nonresonant wavelengths of the harmonic diffractive lens. Calculations of the spatial paraxial field for each wavelength are straightforward. Because the optic is radially symmetric, the calculations are one dimensional in the polar radial coordinates. Calculations are based on the Rayleigh-Sommerfeld approximation,<sup>8</sup>

$$U(P_0, \lambda_i) = \frac{-i}{\lambda_i} \iint_{\Sigma} U(P_1, \lambda_i) \frac{\exp(iks)}{s} r dr d\theta, \quad (7)$$

where the subscript on wavelength denotes a single quasi-monochromatic component. We introduce the standard paraxial approximation

$$s \approx z + \frac{r^2}{2z} \cos(\theta - \varphi) + \frac{r^2}{2z},$$

where the coordinate system is shown in Fig. 6. Following this procedure, the radial variation in amplitude at a fixed axial plane is given by a scaled Hankel transform of the aperture phase function. The transform is evaluated numerically for each discrete wavelength.

We are also interested in the axial distribution of energy as a function of wavelength. The axial amplitude (i.e., at  $\theta = 0$ ) is efficiently found by the introduction of a change of variables,

$$\xi = r^2, \quad d\xi = 2r dr,$$

to convert the axial distribution of amplitude to a scaled Fourier transform of the quadratically scaled radial aperture function.

The numerical simulation presented here is selected to represent the lens experimentally tested, as described in Section 4. The lens is 6 mm in diameter with a power of 34.75 diopters and  $m = 21$  at a design wavelength of 550 nm. The lens is made of acrylic with a sodium *d*-line refractive index of 1.49 and an Abbe dispersion index of 57.4. The resultant lens (thickness is 23.4  $\mu\text{m}$ ). Figure 7 shows the axial distribution of intensity as a function of wavelength between 500 and 640 nm. Only a portion of the

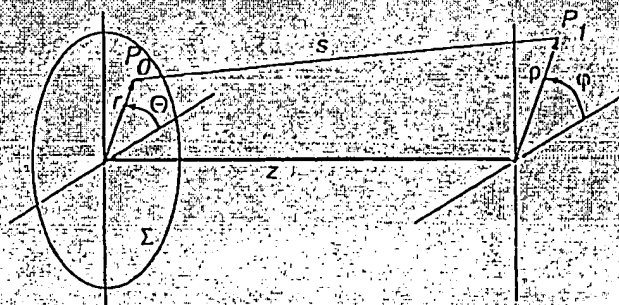


Fig. 6. Coordinate system used in the simulation.

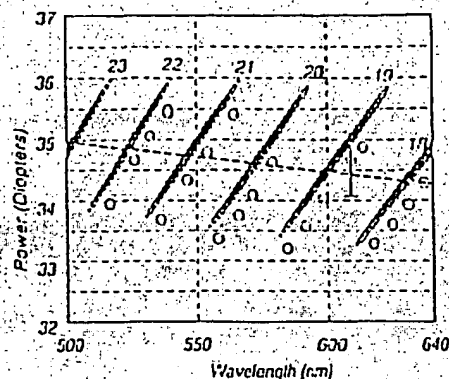


Fig. 7. Numerical simulation of the energy distribution for a 34.75-diopter, 6-mm-diameter lens between 500 and 640 nm. Diffracted orders 18-23 are labeled. The circles represent experimental measurements of focal length.

visible spectrum is shown to reveal more detail. Diffracted orders 18-23 are labeled in the figure.

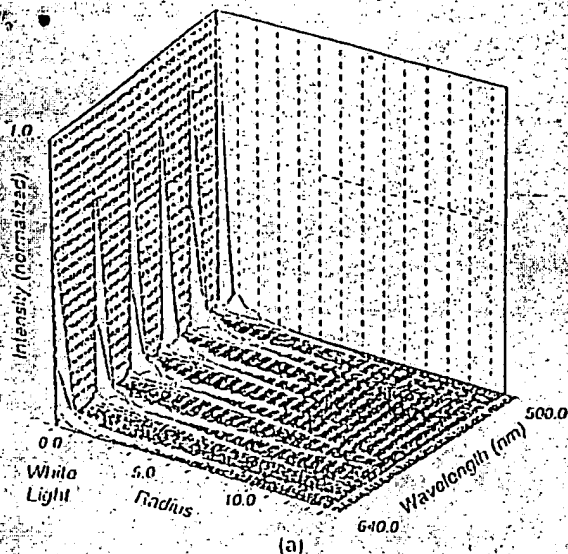
The bold dashed line in Fig. 7 denotes the optical power of a simple refractive acrylic lens. The slope of the line is due to the material dispersion of acrylic ( $V_d = 57.4$ ). Dispersion affects the harmonic diffractive lens in the same way it affects the simple lens. The material dispersion can also be corrected by the use of the diffractive hybrid optics approach. For example, the contribution of material dispersion can be corrected by the superimposition of a second, positive-power simple diffractive lens ( $m = 1$ ) onto the harmonic diffractive lens. This superposed diffractive lens has the full dispersion normally associated with diffractive optics as given in Eq. (1) and opposed to the material dispersion. Sufficient power is added to cancel the material dispersion.

Figure 8 shows the impulse response and the associated diffractive MTF as a function of wavelength. The MTF calculations are for the axial plane associated with the focus at the design wavelength. The locations of the harmonic wavelengths are obvious. At these wavelengths the MTF is diffraction-limited except for the defocus contribution that is due to material dispersion.

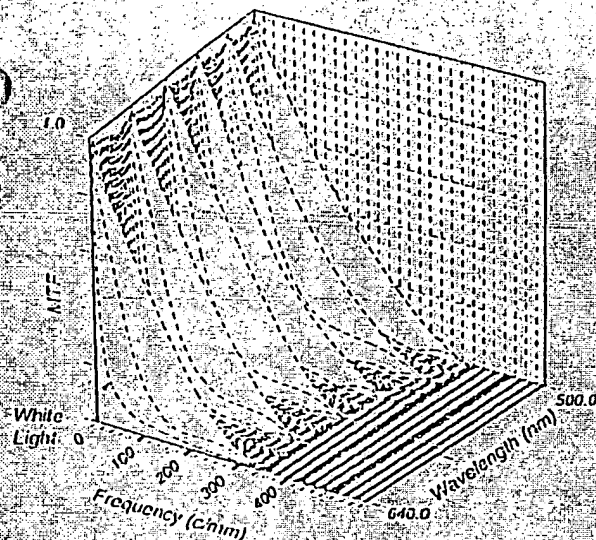
The computational methods used here generate an impulse response and a MTF that include the effects of all diffracted orders; this includes spurious orders that focus in planes other than the nominal image plane. Buralli and Morris<sup>9</sup> define the so-called integrated efficiency to quantify the impact of these spurious diffracted orders. These spurious orders produce a limiting value for the MTF. Both the simulations and the experimental results for impulse response and MTF presented here include these effects.

It is interesting to note that the peaks of the impulse response are narrow because this is a resonance process. One can use the regularity of the impulse response structure of the harmonic diffractive lens to advantage by filtering the broadband illumination so that it contains only components





(a)



(b)

Fig. 8. (a) Impulse response, (b) associated MTF for the 34.75-diopter lens as a function of wavelength. The radial coordinate in (a) is normalized by the Rayleigh resolution; for this particular example it corresponds to  $0.14 \mu\text{m}$ .

suitably close to the harmonic wavelengths. The harmonic lens performance is linearly improved with the fraction of the nonharmonic light filtered. If half of the light is filtered, the chromatic spread is halved, and the MTF at nonzero frequencies approximately doubles.

#### 4. Fabrication Methods

Any method for generating diffractive optics can be used to generate harmonic diffractive lenses. We have used both lithographic (i.e., binary diffractive optics) and diamond turning of a master followed by molding. If the profile is represented by discrete levels, there must be at least two phase levels for each  $2\pi$  phase variation at the shortest wavelength that illuminates the optic. For example, to attain a diffraction efficiency of 80% at 400 nm, the lens in the

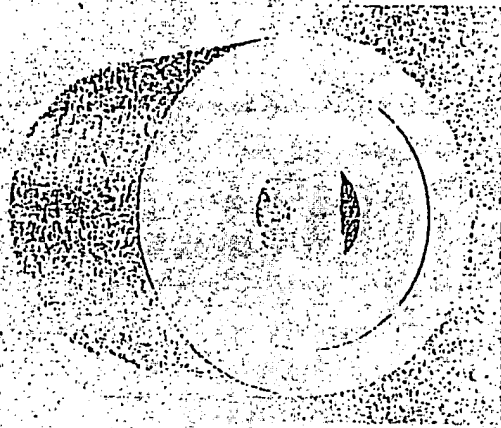


Fig. 9. Diamond-turned aluminum harmonic diffractive lens master. The lens is 6 mm in diameter, and it has 14 zones and a total modulation depth of  $23 \mu\text{m}$ .

previous section would require over 110 discrete levels.

Diamond turning offers the advantage that the continuous groove profile is easily generated. Although diamond turning has difficulty with narrow grooves (standard tool tips are 20 to  $40 \mu\text{m}$  in radius), as  $m$  increases, the narrowest groove width increases proportionally. The standard spherical-tip tool can be replaced with a cleaved or zero-radius tool to resolve the groove profile but with an accompanying increase in scattering from the machined surface.

In the example presented here we have generated an acrylic lens ( $n = 1.494$ ) with a power of 34.75 diopters in air at the design wavelength of 550 nm. Using  $m = 21$  leads to a discrete step size of  $23.4 \mu\text{m}$ . Figure 9 is a photograph of the diamond-turned aluminum master. Materials used to cast lenses from the master include acrylic, photopolymers, and silicone. Figure 10 shows an injection-molded acrylic lens held over a U.S. one-dollar note to show the image detail qualitatively.

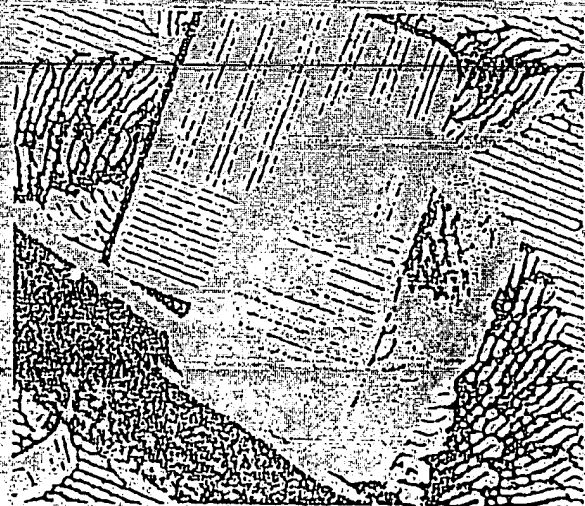


Fig. 10. View of the injection-molded acrylic lens held over a U.S. one-dollar note.

Quality lenses were also created by an open casting technique. First, a mold-release agent was coated onto the mold; the car wax, Finish 2001,<sup>10</sup> worked well with an aluminum mold. A small amount of optical material was placed on the mold and covered with a microscope slide to provide a flat backing. As an optical material, such as acrylic cured, the slide was free to move toward the mold to accommodate shrinkage. The objective was to let shrinkage change the thickness of the lens substrate without affecting the lateral dimension of the lens. Subsequent measurements of the dimensions of the lens with a stylus profilometer showed the lateral dimensions to be unaffected to within a fraction of 1%.

### 5. Imaging Results

The focal length of the harmonic diffractive lens described above was measured at 22 discrete wavelengths between 500 and 640 nm. Light from a xenon arc lamp was spectrally dispersed with a diffraction grating. Entrance and exit slits in our simple monochromator selected the wavelength and the bandwidth. The bandwidth was approximately 5 nm, and the central wavelength could be measured to within 1 nm. The small circles in Fig. 7 indicate these data points. As a result of uncertainties in determining the exact collimation of the broadband source, the measurements of focal lengths have a systematic uncertainty of  $\pm 1.5\%$ .

The lenses were also tested in an Ealing Solid-State EROS MTF instrument. There are a number of optical factors that have an impact on the MTF. Some of these effects are included in the measurements and some are not. The dominant effects are (1) Fresnel reflection losses from the uncoated surfaces, (2) scattering losses from the machining marks, (3) spurious (misfocused) diffracted orders, (4) geometric aberrations, (5) spectral averaging that is due to the finite spectral bandwidth of the source, and (6) resolution of the MTF sensor in the frequency domain.

The reflection losses and the scattering losses are not included in these measurements. In our particular situation, one can estimate these effects based on Fresnel reflection losses of 8%–10% and an rms surface roughness measurement of  $\sim 150$  Å. As described in Section 4 and by Buralli and Morris,<sup>2</sup> a necessary condition to measure the true MTF is to collect all the orders diffracted by the lens. The optical system was arranged to collect at least 90% of the diffracted light. In the most stressing arrangement, the two strongest orders contain nominally 81% of the diffracted energy, and the next two contain 18%. The optical system collects all of the two strongest orders and over half of the two weaker orders. Geometric aberrations are inherently included in the experimental measurement. We worked nominally on the optical axis so only spherical aberrations are present. The optical source for the MTF measurements has a bandwidth of  $\sim 2$  nm, which is not narrow enough to satisfy the quasi-monochromatic condition. This has an effect of

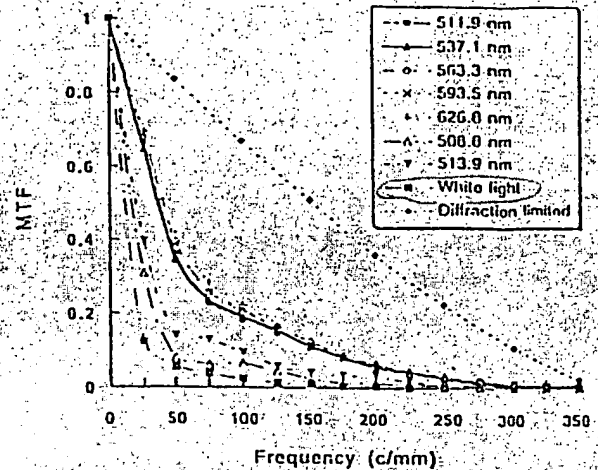


Fig. 11. Measured MTF of the replicated harmonic diffractive lens at several discrete wavelengths and with white light. The curves at 511.9, 537.1, 563.3, 593.5, and 626.8 nm are all at resonant wavelengths. Although the curves are labeled only at increments of 25 cycles/mm, the resolution in the frequency plane is 3 cycles/mm.

spectral averaging that lowers the MTF. Finally, the MTF instrument was configured to have a frequency plane resolution of  $\sim 3$  cycles/mm.

The 34.75-diopter, 6-mm-diameter lens has an effective  $f$ -number of 4.8. The diffraction-limited cutoff frequency of the lens is 350 line pairs/mm at 550 nm. The MTF for an infinite conjugate, axial field point was recorded at a number of wavelengths from 500 to 640 nm with a bandwidth of 2 nm. The variation in the MTF with wavelength follows that shown in Fig. 8. Figure 11 shows representative MTF traces at seven discrete wavelengths and for white light. Five resonant wavelengths and two nonresonant wavelengths are shown. The figure also shows the measured white-light MTF and the diffraction-limited MTF for on an  $f/4.8$  lens at 550 nm.

### 6. Discussion

The harmonic diffractive lens at one extreme is a simple diffractive lens and at the other extreme is a simple refractive lens. We have pointed out some of the advantages and the unique properties of this lens when it is used with either discrete resonant wavelengths or with white light. As we have stated, in general the lens has properties of both diffractive and refractive lenses. The cut locations generated by the modulus operator in Eq. (2) generated the diffractive behavior of the lens. These locations generated the diffracted orders depicted in the top panel of Fig. 2 and are strictly diffractive characteristics that are independent of the refractive index or blazing of the lens. The coupling of energy into each order, however, as represented in the bottom panel of Fig. 2, does depend on the refractive characteristics of blazing, refractive index, and dispersion of the lens.

The harmonic diffractive lens can be used to form images in white light. As the lens becomes thicker





Fig. 12. Monochrome reproduction of an outdoor scene originally recorded on color film.

(i.e., as  $m$  increases), the polychromatic performance of the lens will improve. Figure 12 is a monochrome reproduction of a outdoor scene recorded originally on Kodak VPS color film. The harmonic diffractive lens just discussed was the only optical element in the system. The figure provides qualitative evidence of the image-forming capability of the lens. When the harmonic diffractive lens is used in white light (as opposed to discrete wavelengths) the impulse response and the MTF are averages over the wavelength spectrum. Figures 8 and 11 show the impulse and MTF averages for white light. Computationally, we obtained the results in Fig. 8(b) by integrating the monochromatic MTF across the visible spectrum (with uniform weight in this example). The MTF has a strong zero-frequency component that limits the values of the nonzero frequency components. This effect limits the contrast of white-light images. The degraded contrast of the color version of Fig. 12 is noticeable on inspection, although casual observers tend to miss the effect. As the lens is made thicker (i.e., as  $m$  is increased), the diffractive spreading of each order is reduced, and the lens approaches the refractive situation in which material dispersion dominates the chromatic aberrations.

Another characterization of the white-light performance of the lens is the encircled energy. Figure 13 compares the encircled energy for various  $f/4.8$ , 6-mm-diameter lenses. For reference, the figure shows the limiting cases of a simple diffractive lens (curve d) and a dispersion-free refractive lens (curve a). Basically, for the example shown, the harmonic diffractive lens with  $m = 30$  matches the polychromatic performance of a refractive singlet lens made of acrylic.

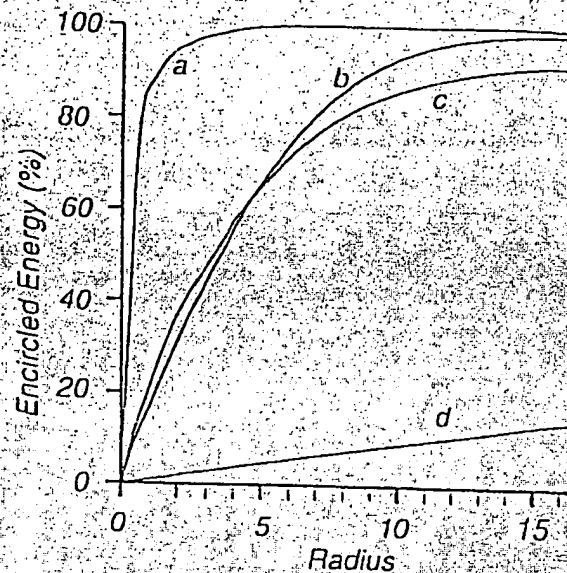


Fig. 13. Polychromatic encircled energy plot for various  $f/4.8$  lenses with 6-mm diameter. The radial coordinate is normalized by the Rayleigh resolution at 550 nm. The spectral band is from 450 to 700 nm. The four curves are (a) a dispersion-free refractive lens, (b) a refractive lens made of acrylic with  $V_d = 57$ , (c) a harmonic diffractive lens with  $m = 30$ , and (d) a simple diffractive lens (i.e.,  $m = 1$ ). The lenses are free of all third- and higher-order aberrations.

The authors acknowledge June Yu for her measurements of the MTF and the focal lengths, and John Toepfen, for producing the replicated optics and recording the outdoor color scene.

#### References

1. D. W. Sweeney and G. Sommargren, "Single element achromatic lens," in *Diffractive Optics*, Vol. 11 of 1994 OSA Technical Digest Series (Optical Society of America, Washington, D.C., 1994), pp. 26-29.
2. G. M. Morris and D. Faklis, "Achromatic and apochromatic diffractive singlets," in *Diffractive Optics*, Vol. 11 of 1994 OSA Technical Digest Series (Optical Society of America, Washington, D.C., 1994), pp. 53-56.
3. M. W. Farn and J. W. Goodman, "Diffractive doublets corrected at two wavelengths," *J. Opt. Soc. Am.* **8**, 860-867; see also M. W. Farn, "Design and fabrication of binary diffractive optics," Ph.D. dissertation (Stanford University, Stanford, Calif., 1990).
4. G. J. Swann, "Binary optics technology: the theory and design of multi-level diffractive optical elements," DARPA Tech. Rep. 854 (Defense Advanced Research Projects Agency, Washington, D.C., 1989).
5. D. A. Buralli and G. M. Morris, "Design of a wide field diffractive landscape lens," *Appl. Opt.* **28**, 3950-3959 (1989).
6. S. J. Bennell, "Achromatic combinations of hologram optical elements," *Appl. Opt.* **15**, 542-545 (1976).
7. W. C. Sweatt, "Achromatic triplet using holographic optical elements," *Appl. Opt.* **16**, 1390-1391 (1977).
8. J. W. Goodman, *Introduction to Fourier Optics* (McGraw-Hill, New York, 1968).
9. D. Buralli and G. M. Morris, "Effects of diffraction efficiency on the modulation transfer function of diffractive lenses," *Appl. Opt.* **31**, 4389-4396 (1992).
10. Finish 2001 Car Polish, distributed by Turtle Wax Inc., Chicago, Ill., 60638-6211.